THE UNIVERSITY OF MICHIGAN

COLLEGE OF ENGINEERING
Department of Mechanical Engineering
Heat Transfer and Thermodynamics Laboratory

Quarterly Progress Report No. 1

For the Period October - December 1960

PRESSURIZATION OF LIQUID OXYGEN CONTAINERS

J. A. Clark
H. Merte, Jr.
V. S. Arpaci
M. Starr
P. Fennema
J. Beukema
S. Eshghy
H. Law

ORA Project 04268

under contract with:

NATIONAL AERONAUTICS AND SPACE ADMINISTRATION
GEORGE C. MARSHALL SPACE FLIGHT CENTER
CONTRACT NO. NAS-8-825
HUNTSVILLE, ALABAMA

administered through:

OFFICE OF RESEARCH ADMINISTRATION ANN ARBOR

April 1961

TABLE OF CONTENTS

NOMENCLATURE

A	cross sectional flow area, ft^2
A_o	cross sectional area of container wall, ft^2
c_p	heat capacity of gas, Btu/lbm °F
c_p'	heat capacity of wall, Btu/lbm °F
$D(\delta)$	disturbance function
$\bar{h}_g$	gas space heat transfer coefficient, Btu/hr ft^2 °F
$\bar{h}_o$	ambient heat transfer coefficient, Btu/hr ft^2 °F
I_o	modified Bessel function of first kind zero order
P	inside perimeter of container, ft
P_o	outside perimeter of container, ft
q''	imposed heat flux on container, Btu/hr ft^2
S	$\frac{\bar{h}_g P}{\rho C_p A} \cdot \frac{x}{v}$
$t(x,\theta)$	wall temperature, °F
$T(x,\theta)$	gas temperature, °F
$T_a(\delta)$	ambient temperature, °F
$T_g(\delta)$	inlet gas temperature, °F
T_ℓ	liquid temperature, °F
V	interface velocity, ft/hr
x	axial space coordinate, ft
δ	$\frac{\bar{h}_g P}{\rho' C_p' A_o} (\theta - \frac{x}{v})$
θ	time, hr
ρ	gas density, lbm/ft^3

ρ'	density of container wall material, lbm/ft^3
ϕ	$q''P_o/\bar{h}_g P$
$\Lambda(s,\delta)$	$= \int_o^{\delta} \delta^* \, e^{-\delta^*} \, I_o[2(s\delta^*)^{1/2}] d\delta^*$
$\psi(\eta s, \frac{\delta}{\eta})$	$= \int_o^{\delta/\eta} e^{-\frac{\delta^*}{\eta}} \, I_o[2(s\delta^*)^{1/2}] \, \frac{d\delta^*}{\eta}$
η	$\frac{1}{1+\bar{h}_o P_o/\bar{h}_g P}$
$\psi(s,\delta)$	solution for unit stepwise disturbance
$\pi(s,\delta)$	solution for arbitrary time dependent disturbance

Subscript

m	spatial mean value at $\theta = \frac{120}{3600}$ hr

I. OPTIMIZATION OF PRESSURIZED-DISCHARGE PROCESSES IN CRYOGENIC CONTAINERS

A. EXPERIMENTAL PROGRAM

A thorough study of the performance characteristics of the annular container as an automatically adjusting thermal guard was completed during this quarter. An evaluation of the electrical heating circuit also was made.

The principal objective in incorporating the annular container into the experimental system is to make possible the precise measurement of the heat flux imposed on the test container wall during an experimental run. The function of the annular container, then, is that of providing an automatically matching thermal guard for the test container, so that the temperature at all opposing points on the test and annular containers are very nearly identical at every moment throughtout the discharge interval. To obtain these identical temperatures across the annular space, it is necessary that the same conditions of discharge and heat flux be imposed on the annular container as on the main, or test, container. For this reason, the annular container is hydrualically connected to the main container at both top and bottom by the inlet and discharge lines, and thus the filling, pressurizing, and discharging is accomplished simultaneously in both containers. To impose identical heat fluxes on both containers, heater ribbon is attached with thermo-setting tape to the outside wall of the main container and to the exterior of the inside wall of the annular container. Figures 5 and 6 of Ref. 1 are photographs of the main and annular containers. Figure 8 of the same report is a wiring

diagram of the heater circuits.

As shown in Figs. 9 of Ref. 1, eight thermocouples numbered 9 to 16 are imbedded in the wall of the main container, and four thermocouples numbered 21 to 24 are imbedded in the inside wall of the annular container directly opposite thermocouples 10, 12, 14, and 16 on the main container. The purpose of these four sets of opposed thermocouples is to obtain the temperature of the wall of both containers at the same axial locations during a pressurized-discharge run. By comparing the respective temperature levels, an indication of the performance of the annular container in its function as a thermal guard may be obtained. Figures 1, 2, and 3 of the present report are plots of experimentally obtained main and annular container wall temperatures. It may be observed that the annular container has essentially reduced the temperature difference of the ambient which immediately surrounds the main container to negligible magnitude, particularly for the adiabatic and low heat flux runs. Since these data are the recorded temperatures at the end of discharge, these curves indicate the maximum temperature differences which can occur at any time during an experimental run. Furthermore, the temperature difference which does exist is negligibly small in comparison to the approximate 400°F difference which would exist if the container were exposed to ambient air at 75°F. These results indicate that the annular container has reasonably well fulfilled its desired function of providing a thermal guard for the test container.

As reported in Ref. 1, there are a number of reasons to suspect that the heater ribbon used to impose various heat fluxes on the main container has

a tendency to expand and to physically pull away from the surface of the container. Some indication of this may be observed from a closer inspection and comparison of the experimental plots presented in Figs. 1, 2, and 3. If the heater ribbon is expanding to a great extent as it is being heated, it will be pulling away from the main container and will necessarily be expanding tighter into the annular container. Thus, the annular container wall may be expected to show higher temperatures than the main container wall. It can be observed in Fig. 1, the adiabatic case, that the main wall temperatures are slightly higher than the corresponding annular wall temperatures. In Fig. 2, the 1083 Btu/hr-ft^2 heat flux case, the relative temperature levels of the annular and main container walls are reversed from those in Fig. 1. That is, the temperatures of the annular wall are now slightly higher than the temperatures of the main container wall. Subsequently, in Fig. 3, the 2166 Btu/hr-ft^2 heat flux case, the temperatures of the annular container wall are even higher relative to the temperatures of the main container wall than for the lower heat flux case in Fig. 2. These observations would tend to substantiate the suspicion that the heater ribbon is indeed expanding away from the main container. This is further confirmed by the departure of the wall temperature distributions from the theory for these higher heat flux runs as shown in Figs. 30 and 31 of Ref. 1. The consequence of this is a great uncertainty in the magnitude of the imposed wall heat flux as the electrical power measured would not all pass to the wall as heat. Some of this would cause the heater ribbon to undergo a thermal transient.

On the basis of these observations, it was decided to perform a series of

tests to determine the temperature levels of the heater ribbon relative to the container wall during a number of experimental heat flux runs. Thus, thermocouples were attached directly to the heater ribbon at positions immediately adjacent to the existing main container wall thermocouples numbered 9, 12, 14, and 15. All the subsequent experimental checks on this were performed with the annular container removed to enable visual inspection of the heater ribbon during an actual test. The significant data of three of these runs are tabulated in Table I. Also, Fig. 4 is a plot of the difference in the temperature between the wall and ribbon versus the temperature of the main container wall. While this plot is not complete, it does show a significant difference in wall and ribbon temperature, particularly when the wall temperature is very low. The pulling away of the ribbon was also visually apparent in the form of randomly spaced vertical strips of frost-free areas on the exterior of the container, while the intermediate areas had a layer of frost on them. The frost-free areas also felt warm to the touch relative to the frosted areas.

All this evidence indicates that the heater ribbon is definitely expanding away from the container at various sections, with the result that an indeterminate percentage of the electrical energy cannot be identified as an imposed wall heat flux, but goes instead into merely increasing the internal energy of the heater ribbon with a resulting increase in its temperature.

Since this method of heating cannot precisely identify the imposed heat flux, as required, it was decided to abandon the heater ribbon in favor of some more reliable means. Preliminary investigations are currently being made

TABLE I

Wall Thermocouple Location	q"	t_r	t_w	$t_r - t_w$	Remarks*
t/c No. 15	620	+148.5	+144.4	+ 4.1	1
27-7/8 in. from	1083	- 3.0	-155.0	+152	2
bottom	1083	+ 18.0	-201.0	+219	3
t/c No. 14	620	+177.6	+141	+ 6.6	1
23-7/8 in. from	1083	- 26.0	-180	+154.0	2
bottom	1083	- 11.0	-310	-299.0	3
t/c No. 12	620	+155.4	+147.3	+ 8.1	1
15-7/8 in. from	1083	- 39.0	-216.0	+177.0	2
bottom	1083	- 86.0	-316.0	+230.0	3
t/c No. 9	620	+141.0	+131.0	+ 10.0	1
3-7/8 in. from	1083	+ 6.0	-259	+265.0	2
bottom	1083	+ 40.0	-309	+349.0	3

Nomenclature:

q'' = heat flux in. Btu/hr-ft^2

t_r = ribbon temperature in. °F

t_w = wall temperature in. °F

*Remarks

1. Ambient air in tank; heat flux turned on for 220 sec. Temperature measurements were made at the end of 220 sec.

2. Normal pressurized (50 psia) discharge run with liquid nitrogen. Time of discharge was 87 sec. Temperature measurements were made at end of discharge.

3. A nondischarge run. At the time heat flux was turned on, the liquid nitrogen was 24.7 in. from the bottom of the tank. Heat flux was left on for 250 sec, at which time the liquid nitrogen level was 22.6 in. from the bottom of the tank. Temperature measurements were made at the end of 250 sec.

of the possibility of using a radiant heat source for this purpose.

As a result of this study, the ribbon and thermo-setting tape were removed from the main container. This necessitates using a value of $\rho' C_p'$ for the analysis corresponding to pure aluminum unweighted for heater ribbon, asbestos insulation, etc., and the replotting of the analytical curves of residual mean density versus inlet gas temperature using this new value of $\rho' C_p'$. The theoretical curve for an adiabatic case using this new $\rho' C_p'$ is given in Fig. 5. To check out the modified system experimentally, four adiabatic runs were performed, also shown in Fig. 5. In the near future, more adiabatic runs will be made to obtain points throughout the range of inlet gas temperatures of from -300°F to +100°F.

For the present and the immediate future, work is progressing toward extending the upper range of inlet-gas temperatures to +600°F. Figure 6 is a simplified schematic diagram of the proposed system, some of which is still tentative. The basic changes from the previous system and operation will be the use of a circulation-type heater rather than a boiling-water heat exchanger, and a bleed-off period prior to actual discharge of the container, necessary to obtain a relatively constant inlet-gas temperature. A flow meter will be incorporated into the system to enable the matching of pressurant flow-rates during bleed-off and subsequent discharge. Matching pressurant flow-rates during these two periods is necessary to obtain a constant inlet gas temperature because any change in the pressurant flow-rate when switching from the bleed-off period to the discharge operation will be reflected in an inlet-gas temperature change. To help offset the effect of any

mis-matching which may occur, a packed regenerator will be incorporated into the system. This will consist essentially of a stainless-steel pipe packed with approximately 9000-5/32-in.-diameter stainless-steel ball bearings. Its main function is to provide a large amount of heat capacity in the system. In operation, the regenerator will be charged to the desired inlet-gas temperature by bleeding for a sufficient length of time. When the discharge period begins, the regenerator will serve to level out any change in temperature caused by flow-rate changes. In effect, the regenerator provides the system with what can be thought of as a thermal "flywheel" or thermal "inertia." Most of the necessary calculations are now completed, and it is expected that construction will begin shortly.

B. DYNAMIC ANALYSIS OF THERMAL SYSTEMS HAVING SIMULTANEOUS, TIME-DEPENDENT, MULTIPLE DISTURBANCES

Introduction

In a previous study,[1] the dynamic response of a single-fluid heat exchanger was investigated for simultaneous multiple-step disturbances in the inlet-fluid temperature, the ambient temperature, and/or the heat flux from the ambient. In this present investigation, the previous work is extended to include the effects of time-dependent, simultaneous, multiple disturbances of an arbitrary form of these same quantities.

Inspection reveals that the governing differential equations[1] are linear with respect to any of these disturbances. That is, the resulting solutions are directly proportional to the magnitude of the step disturbance. This linearity of the problem suggests the convenience of the use of the principle

of superposition (Duhamel's Integral[2]) for time-dependent disturbances, as in the present problem.

Analysis

Let $\phi(s,\delta)$ be the solution of the problem for a single unit, stepwise change in any one of the quantities: inlet-fluid temperature, ambient temperature, or ambient heat flux. Here s is a dimensionless distance, and δ a dimensionless time. Assume now that a disturbance is maintained at zero until a certain time $\delta = \delta_1$, and at that instant is changed to a unit value and is maintained at that value thereafter. It may readily be seen that the resulting temperature distribution will be zero when $\delta < \delta_1$, and when $\delta > \delta_1$ will be given by:

$$\pi(s,\delta) = \phi(s,\delta - \delta_1).$$

Here $\delta-\delta_1$ is the time measured from the instant of change. Next, suppose that a disturbance is changed suddenly to the value D(0) when $\delta = 0$, rather than a unit change and held at this value until $\delta = \delta_1$ as indicated in the sketch. At this new time δ_1 it again is suddenly changed by an amount $D(\delta_1)-D(0)$ to the value $D(\delta_1)$ and is kept at that value until $\delta = \delta_2$, then is suddenly changed again at time δ_2 an amount $D(\delta_2)-D(\delta_1)$, and so on.

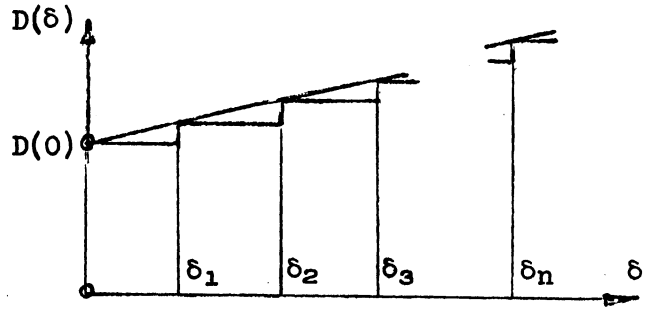

From the linearily of the problem, it may be found that subsequent to the nth time, $\delta = \delta_n$, the temperature distribution is written:

$$\pi(s,\delta) = D(0)\phi(s,\delta) + [D(\delta_1) - D(0)]\phi(s,\delta - \delta_1)$$

$$+ [D(\delta_2) - D(\delta_1)]\phi(s,\delta - \delta_2) + \ldots$$

$$+ [D(\delta_n) - D(\delta_{n-1})]\phi(s,\delta - \delta_n).$$

or

$$\pi(s,\delta) = D(0)\phi(s,\delta) + \sum_{k=1}^{n} \phi(s,\delta - \delta_k)\left(\frac{\Delta D}{\Delta \delta}\right)_k \Delta\delta_k,$$

where

$$\Delta D_k = D(\delta_k) - D(\delta_{k-1}), \quad \Delta\delta_k = \delta_k - \delta_{k-1}.$$

In the limit, as the number n of steps becomes infinite, the definition of integral results in:

$$\pi(s,\delta) = D(0)\phi(s,\delta) + \int_0^{\delta} \phi(s,\delta - \delta^*)\frac{dD(\delta^*)}{d\delta^*}d\delta^*. \qquad (1)$$

This is the classical Duhamel's superposition integral which gives the response of a system to an arbitrary, time-dependent variation in a disturbance $D(\delta)$ in terms of $\phi(s,\delta)$, which is the solution to a unit, stepwise disturbance. By using the method of integration by parts an alternative form may be obtained as:

$$\pi(s,\delta) = D(0)\phi(s,\delta) + \phi(s,\delta - \delta^*)D(\delta^*)\Big|_{\delta^* = 0}^{\delta^* = \delta}$$

$$- \int_0^\delta D(\delta^*)\frac{\partial\phi(s,\delta-\delta^*)}{\partial\delta^*}\, d\delta^*,$$

or, noting that

$$\frac{\partial\phi(s,\delta-\delta^*)}{\partial\delta^*} = - \frac{\partial\phi(s,\delta-\delta^*)}{\partial\delta}$$

we have:

$$\pi(s,\delta) = \phi(s,0)D(\delta) + \int_0^\delta D(\delta^*)\frac{\partial\phi(s,\delta-\delta^*)}{\partial\delta}\, d\delta^*. \qquad (2)$$

In the solution of a linear problem subject to a variable disturbance $D(\delta)$, one of the foregoing integral formulas, Eqs. (1) or (2) can readily be used. Equation (2), however, appears to be more convenient for the present study, and is used here. The same formula, by using its convolutive property,[3] can be rearranged as follows:

$$\pi(s,\delta) = D(\delta)\phi(s,0) + \int_0^\delta D(\delta - \delta^*)\frac{\partial\phi(s,\delta^*)}{\partial\delta^*}\, d\delta^*. \qquad (3)$$

The effect of simultaneous, multiple, time-dependent disturbances of an arbitrary form may then be obtained by the combination from the following three problems.

Case I - Time-Dependent Inlet Temperature Only.—The response of the fluid and wall temperatures to a step change at the inlet-fluid temperature is given in the previous study[1b] [Eqs. (29), (30)]. The results which cor-

respond to $\phi(s,\delta)$ in this present notation, for

$$\delta \equiv \frac{\bar{h}_g P}{\rho' C'_p A_o}\left(\theta - \frac{x}{v}\right) \geq 0,$$

are

$$\frac{T(s,\delta,\eta) - T_\ell}{T_g - T_\ell} = e^{-s}\left\{\psi(\eta s,\delta/\eta) + e^{-\frac{\delta}{\eta}} I_o\left[2(s\delta)^{1/2}\right]\right\}, \qquad (4)$$

and

$$\frac{t(s,\delta,\eta) - T_\ell}{T_g - T_\ell} = \eta e^{-s}\,\psi(\eta s,\delta/\eta), \qquad (5)$$

in which η is a dimensionless parameter defined in the nomenclature. Defining the time-dependent inlet-fluid temperature as $T_g(\delta)-T_\ell = [T_g-T_\ell]D(\delta)$, substituting Eqs. (4) and (5) into Eq. (3), and rearranging gives:

$$\frac{T(s,\delta,\eta) - T_\ell}{T_g - T_\ell} = e^{-s}\left[D(\delta) + \int_o^\delta D(\delta - \delta^*)e^{-\frac{\delta^*}{\eta}} \frac{\partial I_o\left[2(s\delta^*)^{1/2}\right]}{\partial \delta^*} d\delta^*\right], \quad \delta \geq 0 \qquad (6)$$

and

$$\frac{t(s,\delta,\eta) - T_\ell}{T_g - T_\ell} = e^{-s}\int_o^\delta D(\delta - \delta^*)e^{-\frac{\delta^*}{\eta}} I_o\left[2(s\delta^*)^{1/2}\right] d\delta^*, \quad \delta \geq 0 \qquad (7)$$

Case II - Time-Dependent, Moving Ambient Only.—The response of the fluid and wall temperatures to a step change in the moving ambient temperature has been given in Ref. 1b [Eqs. (48), (49)]. The results for $\delta \geq 0$ are:

$$\frac{T(s,\delta,\eta) - T_\ell}{T_a - T_\ell} = 1 - e^{-s}\,\psi(\eta s,\delta/\eta) - e^{-(1-\eta)\frac{\delta}{\eta}}\left[1 - e^{-s}\,\psi(s,\delta)\right], \qquad (8)$$

and

$$\frac{t(s,\delta,\eta) - T_\ell}{T_a - T_\ell} = (1-\eta) + \eta\left[1 - e^{-s}\,\psi(\eta s,\delta/\eta)\right] - e^{-(1-\eta)\frac{\delta}{\eta}}\left[1 - e^{-s}\,\psi(s,\delta)\right] \tag{9}$$

Defining the time-dependent, moving ambient temperature as $T_a(\delta)-T_\ell = (T_a-T_\ell)D(\delta)$, substituting Eqs. (8) and (9) into Eq. (3), and rearranging gives:

$$\frac{T(s,\delta,\eta) - T_\ell}{T_a - T_\ell} = \left(\frac{1-\eta}{\eta}\right)\int_o^\delta D(\delta - \delta^*)\left\{e^{-(1-\eta)\frac{\delta^*}{\eta}}\left[1 - e^{-s}\,\psi(s,\delta^*)\right] - e^{-s}\,e^{-\frac{\delta^*}{\eta}}\,I_o\left[2(s\delta^*)^{1/2}\right]\right\}d\delta^*, \quad \delta \geqslant 0 \tag{10}$$

and

$$\frac{t(s,\delta,\eta) - T_\ell}{T_a - T_\ell} = \left(\frac{1-\eta}{\eta}\right)\int_o^\delta D(\delta - \delta^*)\,e^{-(1-\eta)\frac{\delta^*}{\eta}}\left[1 - e^{-s}\,\psi(s,\delta^*)\right]d\delta^*, \quad \delta \geqslant 0 \tag{11}$$

Case III - Time-Dependent, Moving Heat Flux Only.—The response of the fluid and wall temperatures to a step change in the moving heat flux is also given in Ref. 1b [Eqs. (60), (61)]. The results for $\delta \geqslant 0$ are:

$$\frac{T(s,\delta) - T_\ell}{\Phi} = \delta + e^{-s}\,[\Lambda(s,\delta) - (1+\delta)\psi(s,\delta)], \tag{12}$$

and

$$\frac{t(s,\delta) - T_\ell}{\Phi} = \delta + e^{-s}\,[\Lambda(s,\delta) - \delta\psi(s,\delta)], \tag{13}$$

where

$$\Phi = q''P_o/\bar{h}_g P.$$

The time-dependent, moving heat flux is now defined as $\Phi(\delta) = \Phi D(\delta)$. Then substituting Eqs. (12) and (13) into Eq. (3) and rearranging gives:

$$\frac{T(s,\delta) - T_\ell}{\Phi} = \int_o^\delta D(\delta - \delta^*)\left\{[1 - e^{-s}\,\psi(s,\delta^*)]\right.$$
$$\left. -e^{-s}.e^{-\delta^*}\, I_o\left[2(s\delta^*)^{1/2}\right]\right\} d\delta^*, \quad \delta \geq 0 \tag{14}$$

and

$$\frac{t(s,\delta) - T_\ell}{\Phi} = \int_o^\delta D(\delta - \delta^*)[1 - e^{-s}\,\psi(s,\delta^*)]d\delta^*, \quad \delta \geq 0 \tag{15}$$

The foregoing procedure completes the solution of fluid and tube-wall temperatures response corresponding to a single, arbitrary time-dependent disturbance. The solution of two problems which are presently under study can readily be obtained by properly combining two of the three above-mentioned cases. These problems are:

Problem 1: Moving Ambient.—Actually, under the name of "Moving Ambient" two simultaneous disturbances are considered. These are the time-dependent variations in the ambient and inlet fluid temperatures. The solution is the linear combination of Eqs. (6), (10), and (7), (11) which can be written as follows:

$$\frac{T(s,\delta) - T_\ell}{T_g - T_\ell} = e^{-s}\left\{D_1(\delta) + \int_o^\delta D_1(\delta - \delta^*)e^{-\frac{\delta^*}{\eta}} \frac{\partial I_o\left[2(s\delta^*)^{1/2}\right]}{\partial\delta^*} d\delta^*\right\}$$

$$+ \left(\frac{T_a - T_\ell}{T_g - T_\ell}\right)\left(\frac{1-\eta}{\eta}\right)\int_o^\delta D_2(\delta - \delta^*)\left\{e^{-(1-\eta)\frac{\delta^*}{\eta}}\left[1 - e^{-s}\,\psi(s,\delta^*)\right]\right.$$

$$\left. -e^{-s}\cdot e^{-\frac{\delta^*}{\eta}} I_o\left[2(s\delta^*)^{1/2}\right]\right\} d\delta^*, \quad \delta \geqslant 0 \tag{16}$$

and

$$\frac{t(s,\delta) - T_\ell}{T_g - T_\ell} = e^{-s}\int_o^\delta D_1(\delta - \delta^*)e^{-\frac{\delta^*}{\eta}} I_o\left[2(s\delta^*)^{1/2}\right] d\delta^*$$

$$+ \left(\frac{T_a - T_\ell}{T_g - T_\ell}\right)\left(\frac{1-\eta}{\eta}\right)\int_o^\delta D_2(\delta - \delta^*)e^{-(1-\eta)\frac{\delta^*}{\eta}}\left[1 - e^{-s}\,\psi(s,\delta^*)\right]d\delta^*, \quad \delta \geqslant 0 \tag{17}$$

where $D_1(\delta)$ and $D_2(\delta)$ are the different, time-dependent disturbances in the inlet and ambient temperatures, respectively.

Problem 2: Moving Heat Flux.—This problem combines the time-dependent moving heat flux and the inlet-fluid temperatures. The solution is obtained by superimposing Eqs. (6), (14), and (7), (15). The result is:

$$\frac{T(s,\delta) - T_\ell}{T_g - T_\ell} = e^{-s}\left\{D_1(\delta) + \int_o^\delta D_1(\delta - \delta^*)e^{-\delta^*} \frac{\partial I_o\left[2(s\delta^*)^{1/2}\right]}{\partial\delta^*} d\delta^*\right\}$$

$$+ \frac{q''P_o/\bar{h}P}{T_g - T_\ell}\int_o^\delta D_3(\delta - \delta^*)\left\{\left[1 - e^{-s}\,\psi(s,\delta^*)\right]\right.$$

$$\left. -e^{-s}\cdot e^{-\delta^*} I_o\left[2(s\delta^*)^{1/2}\right]\right\} d\delta^*, \quad \delta \geqslant 0 \tag{18}$$

and

$$\frac{t(s,\delta) - T_\ell}{T_g - T_\ell} = e^{-s} \int_o^\delta D_1(\delta - \delta^*) e^{-\delta^*} I_o\left[2(s\delta^*)^{1/2}\right] d\delta^*$$

$$+ \frac{q''P_o/\bar{h}P}{T_g - T_\ell} \int_o^\delta D_3(\delta - \delta^*)[1 - e^{-s}\,\psi(s,\delta^*)]d\delta^*, \quad \delta \geq 0 \tag{19}$$

where $D_1(\delta)$ and $D_3(\delta)$ correspond to time-dependent disturbances in the inlet-fluid temperature and the moving heat flux, respectively. During the next period, examples of these types of systems will be worked out using time-dependent disturbances.

II. BOILING OF A CRYOGENIC FLUID UNDER REDUCED GRAVITY

During this report period, drop tests with a dummy load were made to determine the shock a test package would receive upon striking the buffer piston. A measure of the shock was obtained from the response of a 1000-g piezoelectric accelerometer mounted on the test platform, and a strain-gage-type pressure transducer mounted in the face of the buffer piston. The output signals from these two instruments are displayed on a dual beam oscilloscope and recorded photographically.

Initially a 1-in.-thick, heavy rubber pad was placed on the buffer piston. This resulted in an undesirable high decleration of 250 g's upon impact, as indicated by Fig. 7. By installing a long automotive-type coil spring and the rubber pad on top of the piston, the impact was reduced to 200 g's, shown in Fig. 8. Also shown is the pressure build-up within the buf-

fer cylinder. (The cylinder configuration is shown in Fig. 35 of Ref. 1.) The initial impact, still too high, results from the force required to accelerate the light aluminum cap mounted on top of the spring. The cap is necessary to assure stability of the test platform upon contact.

This impact was reduced further by transmitting the force to accelerate the cap through a block of styrofoam. In the process the styrofoam is crushed and thereby also serves as an additional energy absorber. The impact with the styrofoam could be reduced further by placing on top of the styrofoam a 2-1/2-in. thickness of heavy foam rubber. A number of different combinations of spring length, styrofoam density, and styrofoam thickness were used, the acceleration and pressure-time record of two being shown in Figs. 9 and 10. The optimum configuration consisted of a short spring, plus 1-in. thickness of high-density styrofoam plus 4-in. thickness of low-density styrofoam plus 2-1/2 in. of soft rubber pad. The acceleration and pressure-time results for this combination are shown in Fig. 11, which indicates a maximum impact deceleration of 15 g's with a maximum pressure of 250 psi within the hydraulic cylinder.

Release of the test platform is still being accomplished by melting the support wire electrically, which requires a finite time interval. Since it is necessary to drop the test platform at a precisely predetermined time, the time required to melt the wire link must be reproducible. It was found that spring-loaded current clamps, in conjunction with a constant wire-link length resulted in consistent link-melting time intervals. Oscillograph traces of the melting times for two different link lengths are shown in Fig. 12. A

1/2-in. length has been found to give the minimum burn time of 1.35 sec with the particular material and wire diameter. The release of the platform with this device is essentially instantaneous as shown.

A voltage tap in the release link circuit is transmitted to the Sanborn 4-channel recorder to indicate the exact instant of test platform release. This signal shows the initiation of reduced gravity on the test platform.

The 0- to 1-g accelerometer, which will beused to indicate the fractional gravity value during counterweighted drops, was mounted on the test platform. Its response for a typical 0-g drop test is shown in Fig. 13. The initial overshoot in the response is within that specified for the instrument by the manufacturer and results from the dynamics of its own internal components. The drop time can be determined directly from the oscillographic record and is seen to be 1.4 sec. This compares with the predicted value of 1.40 sec with a total free fall distance of 31 ft 9 in. Also to be noted is that within the sensitivity range of the recording system (better than 0.01 g) no change in the acceleration of the test platform is detected during the free fall period, indicating that the effect of air resistance and friction of the guide wires is negligible.

Since the accelerometer provides no additional information during subsequent zero g tests, it has been removed, and will be used only for counterweighted tests, where accelerations between 0- to 1-g are desired.

To test the concept of using a solid sphere as a calorimeter in a transient boiling process, for the purpose of obtaining heat-transfer coefficients and to test various instrumentation techniques, a 5/8-in.-diameter aluminum

(exact composition unknown) sphere was obtained. A 1/32-in.-diameter hole was drilled to the center to measure the temperature at the center of the sphere. The sphere is supported by a 1/16-in.-diameter, stainless-steel rod inserted into a 1/16-in.-diameter hole in the sphere with a press fit. The low thermal conductivity of stainless steel minimizes errors due to conduction down the support. Figure 14 is a photograph of the sphere.

Initially, a thermocouple was constructed using a 30-gage constantan wire down the center of a 1/32-in.-OD copper tube, with a welded junction at the tip, and a ceramic cement as the insulation. The thermocouple failed at liquid nitrogen temperature due to the differential coefficient of expansion of the copper tube and the constantan wire in conjunction with a rigid cement. A more flexible insulating cement such as Glyptol remedied this problem. To connect a copper wire to the 1/32-in.-diameter copper tube, it was necessary that the tube extend out of the sphere by at least 1/4-in. This in effect acted as a copper fin between the thermocouple junction and the surrounding fluid, with an attendant error in temperature measured with the severe temperature differences present. This manifested itself by the presence of two inflection points in the cooling curve of the system, one for the thermocouple tube itself passing through the transition and nucleate boiling regime, and the other for the test sphere passing through the transition and nucleate boiling regime at a later time.

Two 40-gage copper constantan wires were then substituted for the above thermocouple, with a small soft-soldered junction. To insure good thermal contact between the junction and the sphere metal, a small quantity of Woods

metal is placed in the hole, melted, and the thermocouple inserted. The low melting point of the Woods metal (87°C) causes no deterioration of the enamel insulation of the wires.

A typical cooling curve for the aluminum sphere at 1 g is shown in Fig. 15. The sphere was initially at room temperature and then plunged suddenly into liquid nitrogen. The temperature range covers 70°F to -320°F.

The exponential nature of the temperature in the film boiling region is to be noted, and is as anticipated. The sudden change in temperature toward the latter part of the curve is a consequence of the large heat-transfer rates associated with transitional and nucleate boiling. It is this region that is of primary interest at reduced and zero gravity fields.

Figure 16 shows this same region in a different test with a more expanded time and voltage scale. A Sanborn Model 150-1500 4-channel recorder was used with a low-level preamplifier. It is noted that the change from film boiling to natural convection through the transition and nucleate boiling regimes takes place over a period of approximately one second. Since it is desired to study the transitional and nucleate boiling regimes under reduced gravity, it will be necessary to release the test platform at precise points within this short interval.

From the EMF-time data presented in Fig. 15, a time-temperature curve was constructed, having a form similar to that of Fig. 15. By measuring the slope, $dt/d\theta$, it is possible to calculate the instantaneous value of the film boiling heat-transfer coefficient using Eq. (66) of Ref. 4. This equation assumes a lumped parameter system, which is valid for this system since the

Biot Number is approximately 0.009 in the film boiling region.

The values $\bar{h}$ are shown in Fig. 17 as a function of the sphere temperature minus the fluid temperature, $t_s - t_\ell$. The fluid temperature is essentially the saturation temperature. For comparison, several points are included from Figs. 14-19 of Ref. 5.

Several conditions suggest that these be considered tentative data only. The composition of the aluminum is not known. Hence the values of the specific heat C_p used, shown in Fig. 18 as a function of temperature, may differ from the actual values. Also, the calibration of the 40-gage thermocouple wire was made at only two points, the ice point and the liquid nitrogen temperature existing at the time of the test. Further, in the transition and nucleate boiling regions, the validity of a lumped parameter system cannot be determined since the temperature was measured at only one point.

The short time interval existing during the transition and nucleate boiling regions can be extended by using a sphere of larger-volume-to-surface-area ratio (i.e., a large sphere), or using a material having a larger ρC_p, or both. Accordingly, a sphere one inch in diameter is under construction using electrolytic tough pitch copper. The copper not only has a ρC_p approximately twice that of aluminum, but its thermal properties are better known as a function of temperature. Further, the larger size will permit the insertion of two thermocouples to evaluate better the lumped or nonlumped characteristics. The data obtained will be reported in the next progress report.

An insulated container has been constructed and mounted on the test platform, shown in Fig. 19. For reduced gravity tests the container is filled

with liquid nitrogen, the sphere inserted, and the platform released at a predetermined time.

During the next reporting period, the thermal response of the 1-in.-diameter copper sphere will be determined at 1 g. If it performs satisfactorily, "zero" g tests will then be conducted. It is anticipated that the design and construction of a counterweight assembly for reduced gravity tests will begin.

III. HEAT TRANSFER TO A CRYOGENIC FLUID IN AN ACCELERATING SYSTEM

The assembly of the test vessel and the calibration of the thermocouples have been completed. Three thermocouples are inserted radially in the heater cylinder for measurement of the surface temperature. Upon testing the assembly at liquid nitrogen temperatures, the thermocouples failed.

The thermocouples were constructed using a 1/32-in.-OD copper tube with a constantan wire passing down the center, with a condenser-discharge welded junction at one end. With the rigidity imposed by the ceramic cement used as an electrical insulator between the wire and the tube, the differential coefficient of expansion of the copper and constantan caused the junction to fail. The test vessel was disassembled and the thermocouples replaced with a similar type using "Glyptol" as the insulating cement. This provided sufficient flexibility to allow for the differential expansions encountered.

Differential expansions also caused failure of the Teflon seal between the vessel side walls and the bottom assembly. This difficulty has been overcome by having the test vessel partially cooled down before final tightening

of the assembly.

A liquid level float has been installed and actuates two microswitches for remote indicators.

During the next period a series of tests will be conducted using liquid nitrogen at 1 g to determine the characteristics of the system. Different measuring techniques and systems will be used. It is anticipated that, because of the varying liquid depth due to boil-off, some type of a recording instrument will be required for the measurement of temperatures, with an attendent loss of accuracy. The extent to which this can be tolerated is not evident at this point, and will require preliminary measurements under condition of high force fields.

REFERENCES

1a. V. S. Arpaci, J. A. Clark, and W. O. Winer, "Dynamic Response of Fluid and Wall Temperatures During Pressurized-Discharge of a Liquid from a Container," Advances in Cryogenic Engineering, Vol. 6, 1961.

1b. J. A. Clark, H. Merte, V. S. Arpaci, and others, Pressurization of Liquid Oxygen Containers, ORA Report 03583-3-F, Univ. of Mich., Ann Arbor, March, 1961.

2. H. S. Carslaw, and J. C. Jaeger, Conduction of Heat in Solids, 2nd Edition, Oxford, 1959.

3. R. V. Churchill, Modern Operational Mathematics in Engineering, McGraw-Hill Book Co., Inc., New York, 1944.

4. J. A. Clark, H. Merte, V. S. Arpaci, and others, UMRI Report 03583-2-P, Univ. of Mich., Ann Arbor, August, 1960.

5. W. H. McAdams, Heat Transmission, McGraw-Hill Book Co., Inc., New York, 1954.

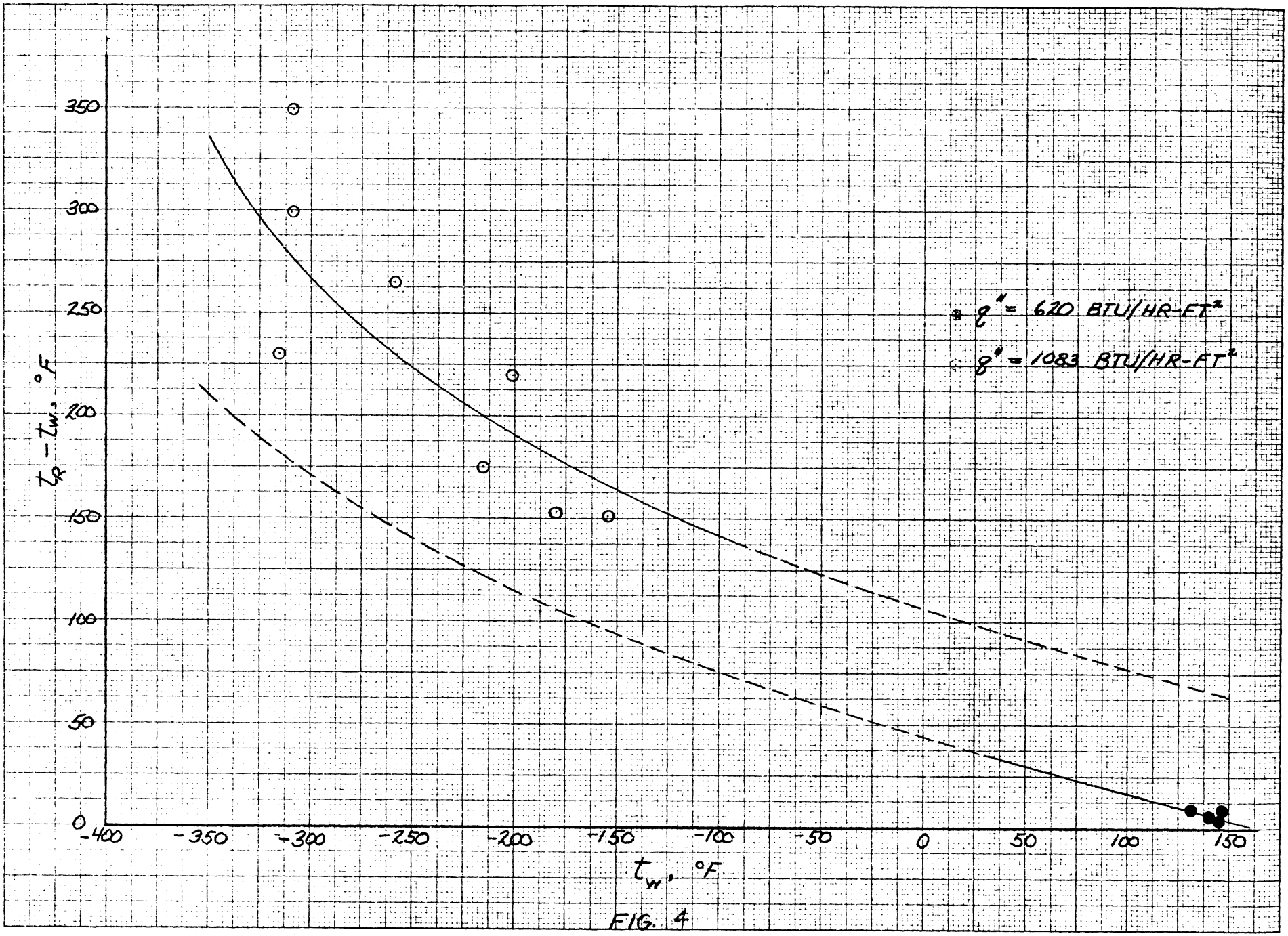
$t_R - t_w$, °F
350
300
250
200
150
100
50
0
-400
-350
-300
-250
-200
-150
-100
-50
0
50
100
150
t_w, °F
$q'' = 620$ BTU/HR-FT²
$q'' = 1083$ BTU/HR-FT²

FIG. 4

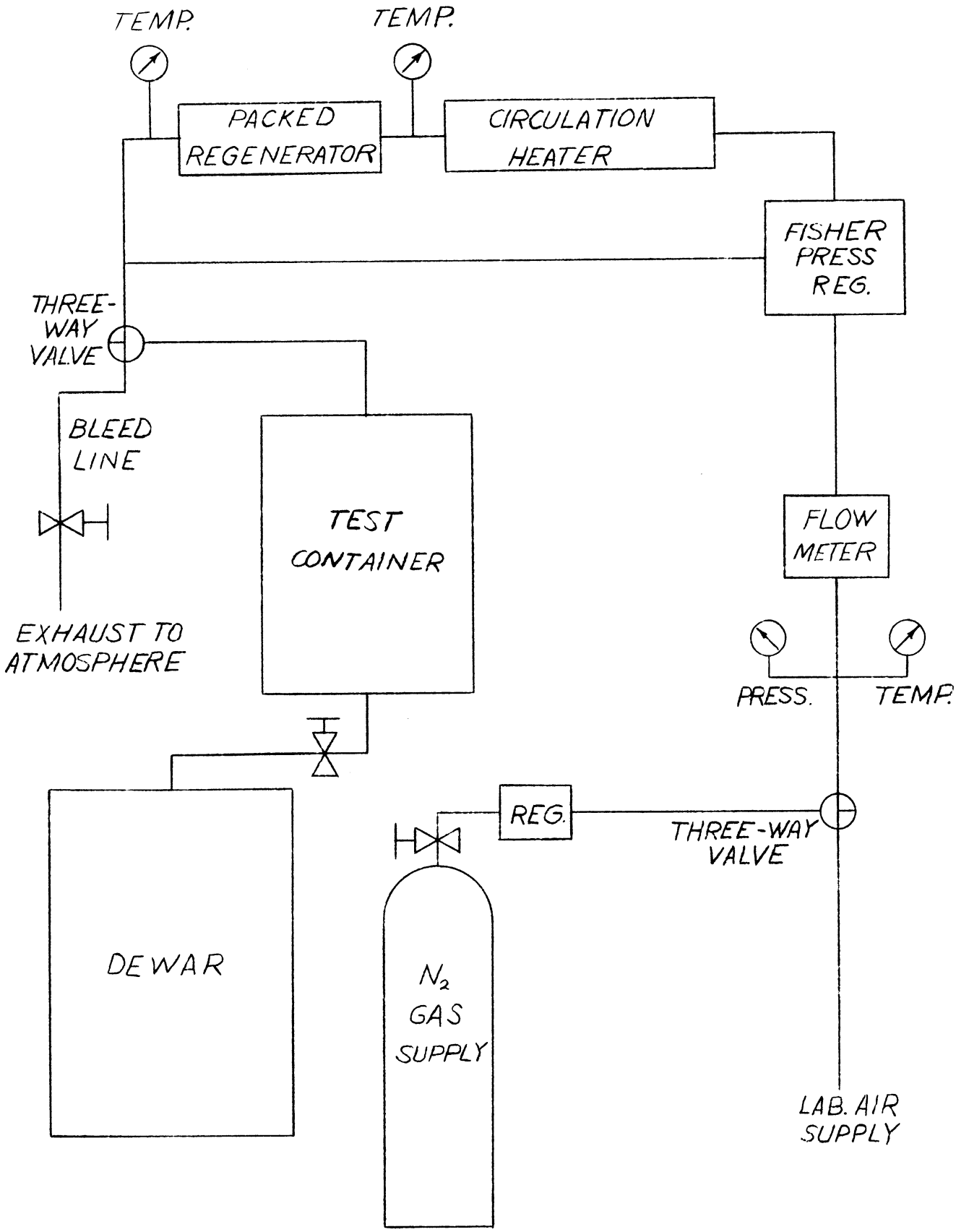

PROPOSED HIGH TEMPERATURE INLET GAS SYSTEM
FIG. 6

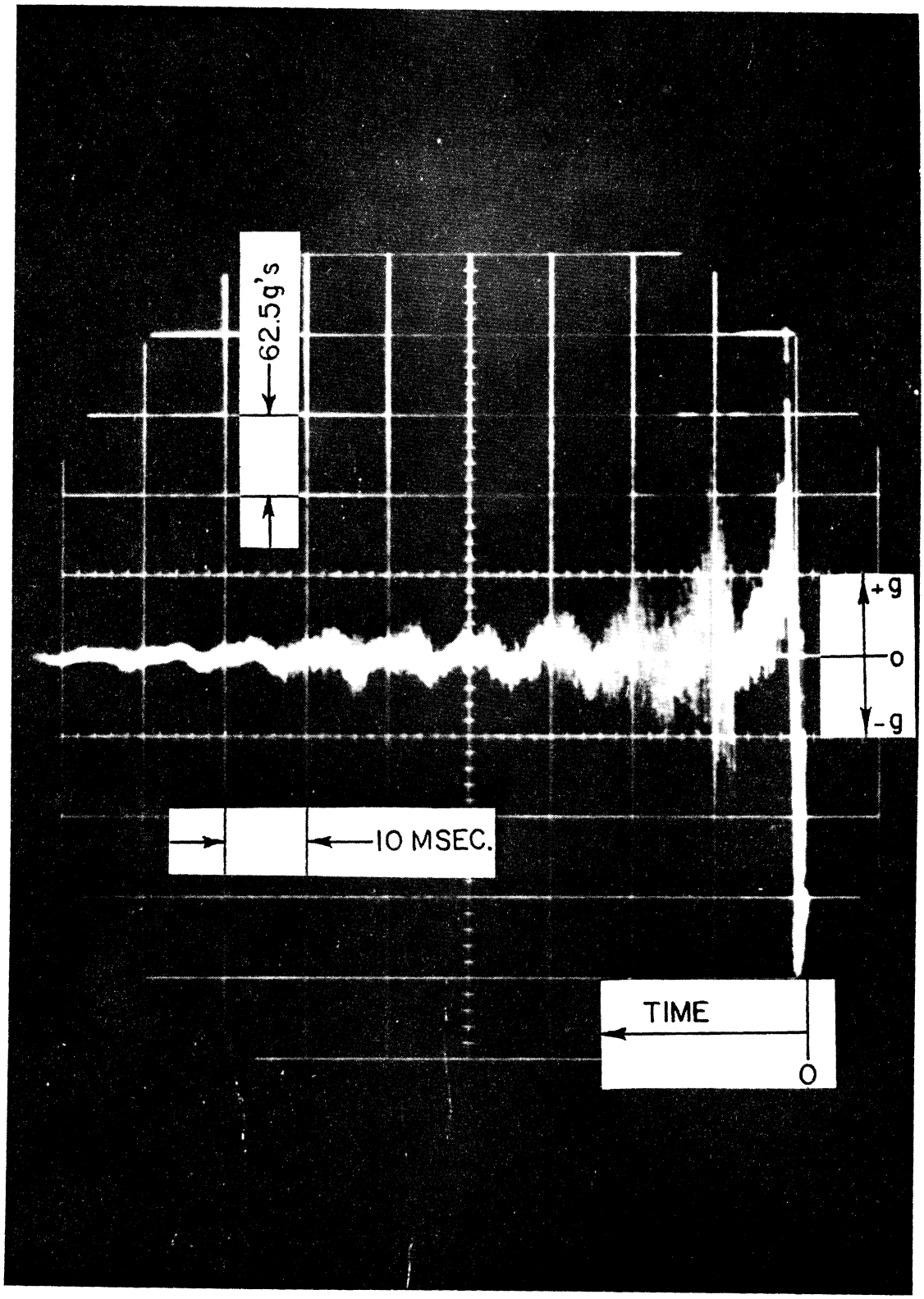

Fig. 7. Impact deceleration of test platform with 1-in.-thick heavy rubber pad on buffer piston.

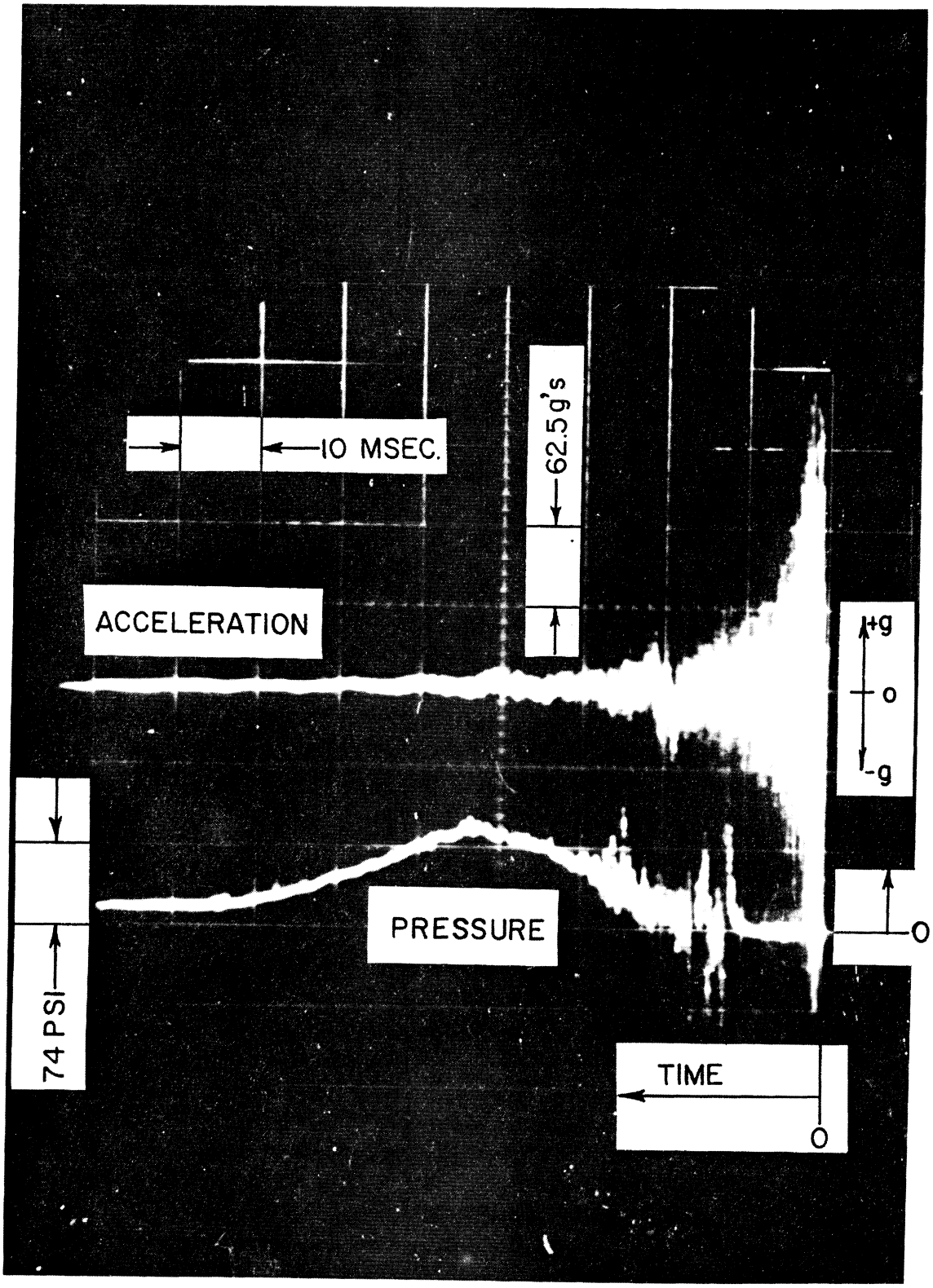

Fig. 8. Deceleration of test platform and pressure buildup in buffer cylinder with long coil spring and 1-in.-thick rubber pad.

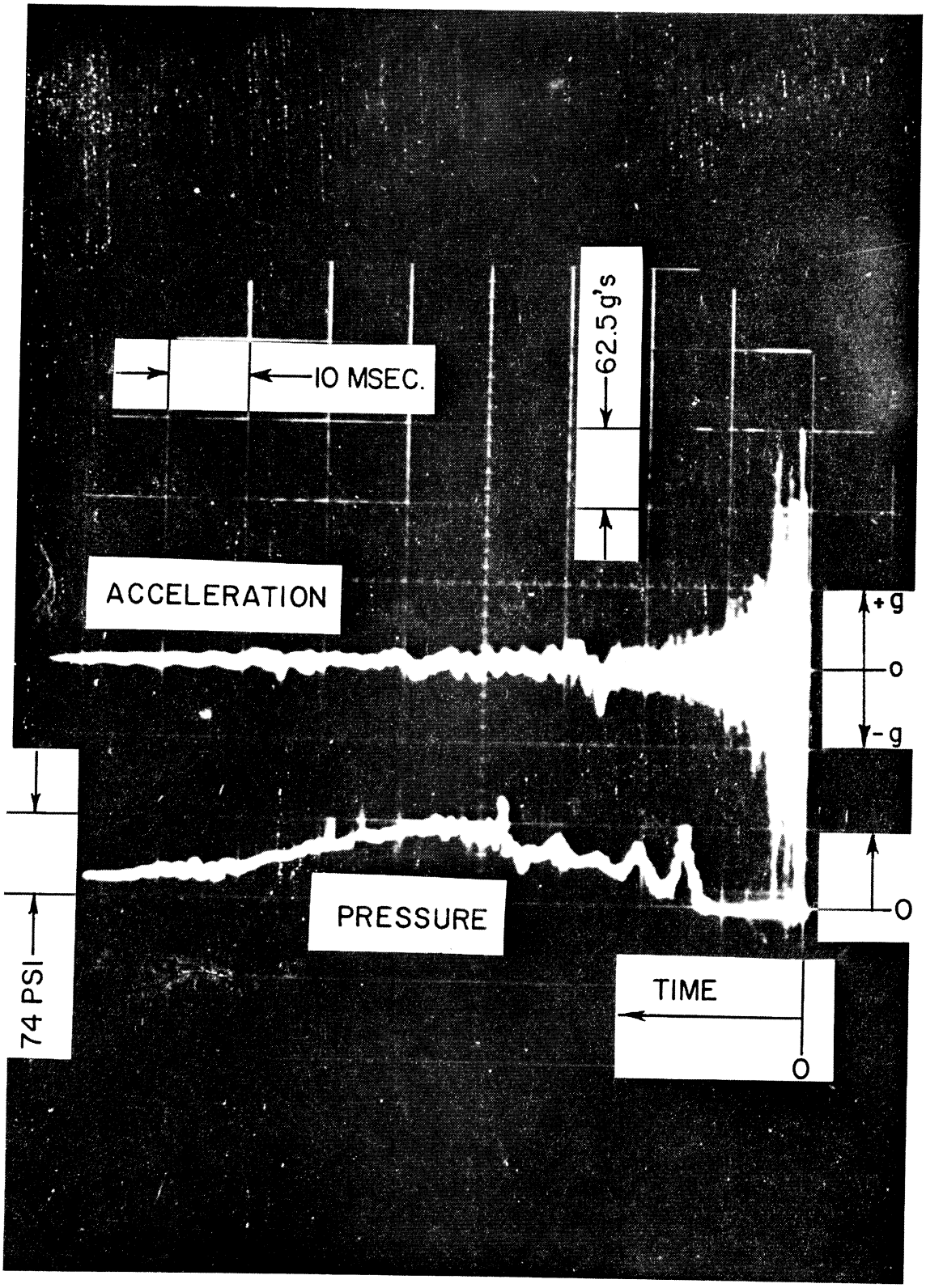

Fig. 9. Deceleration of test platform and pressure buildup in buffer cylinder with long coil spring and 4-in. low-density styrofoam.

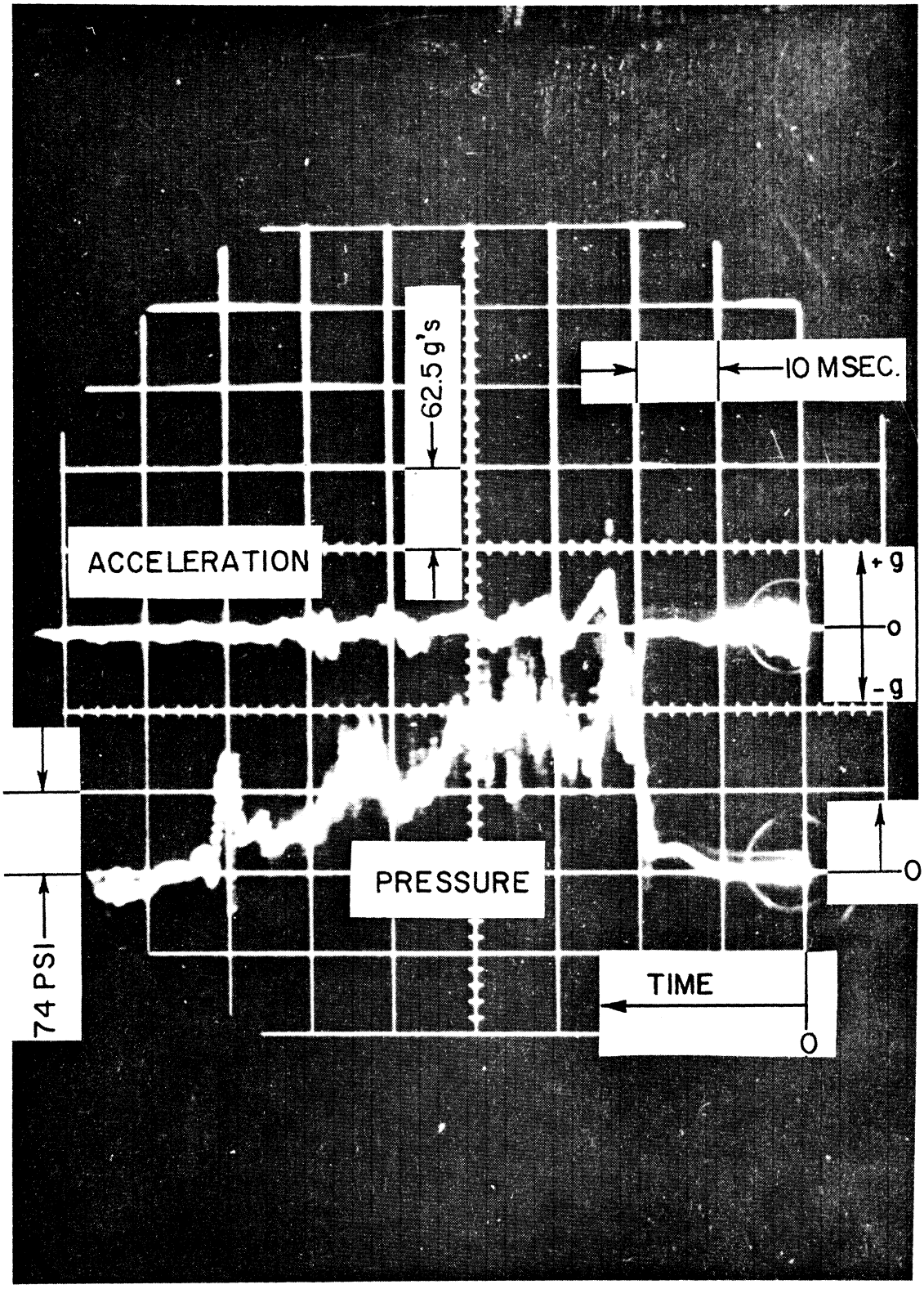

Fig. 10. Deceleration of test platform and pressure buildup in buffer cylinder with short spring, 4-in. low-density styrofoam and 1-3/4-in. soft rubber.

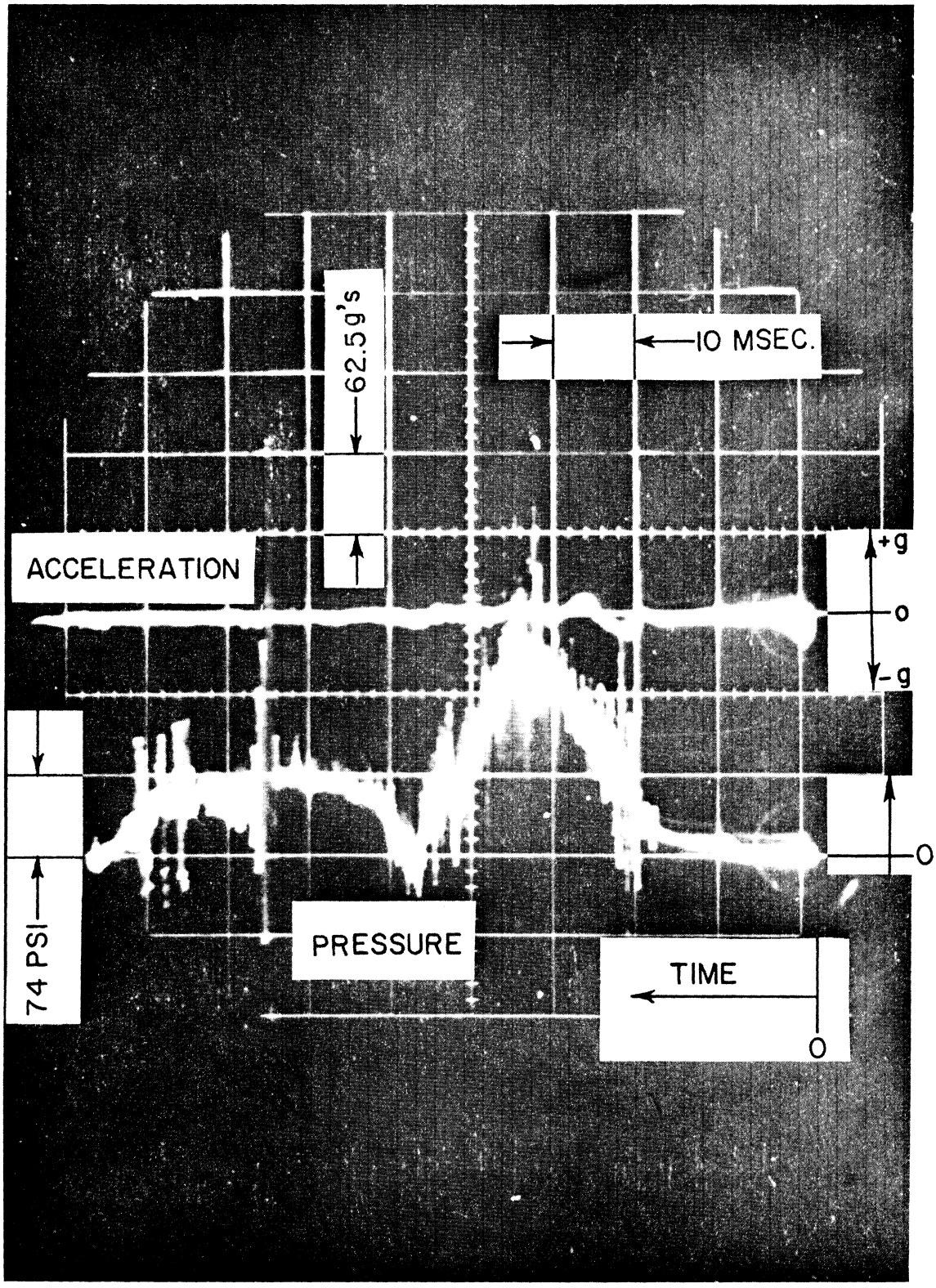

Fig. 11. Deceleration of test platform and pressure buildup in buffer cyclinder with final configuration.

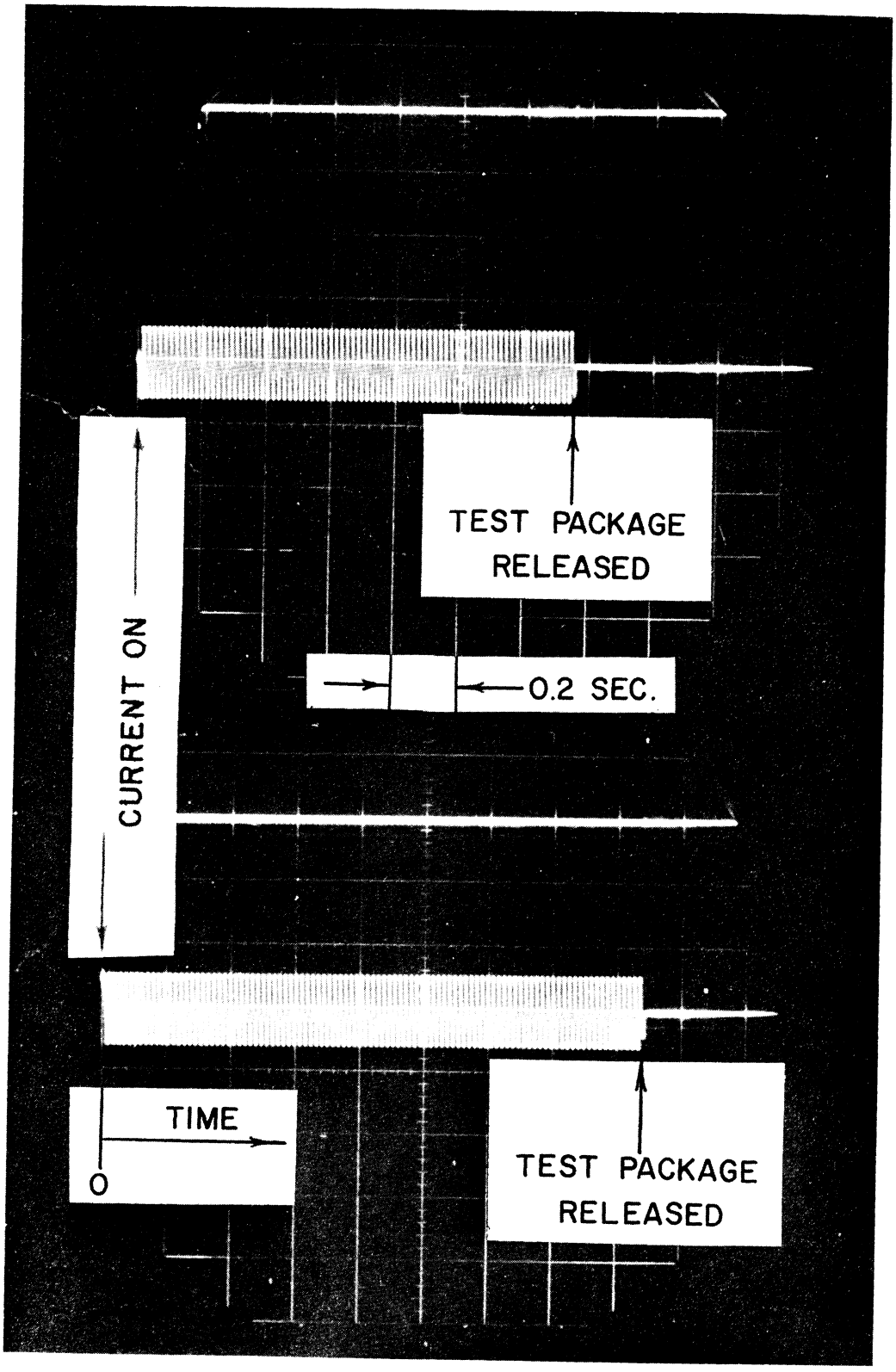

Fig. 12. Oscillographic record of time required to melt release link.

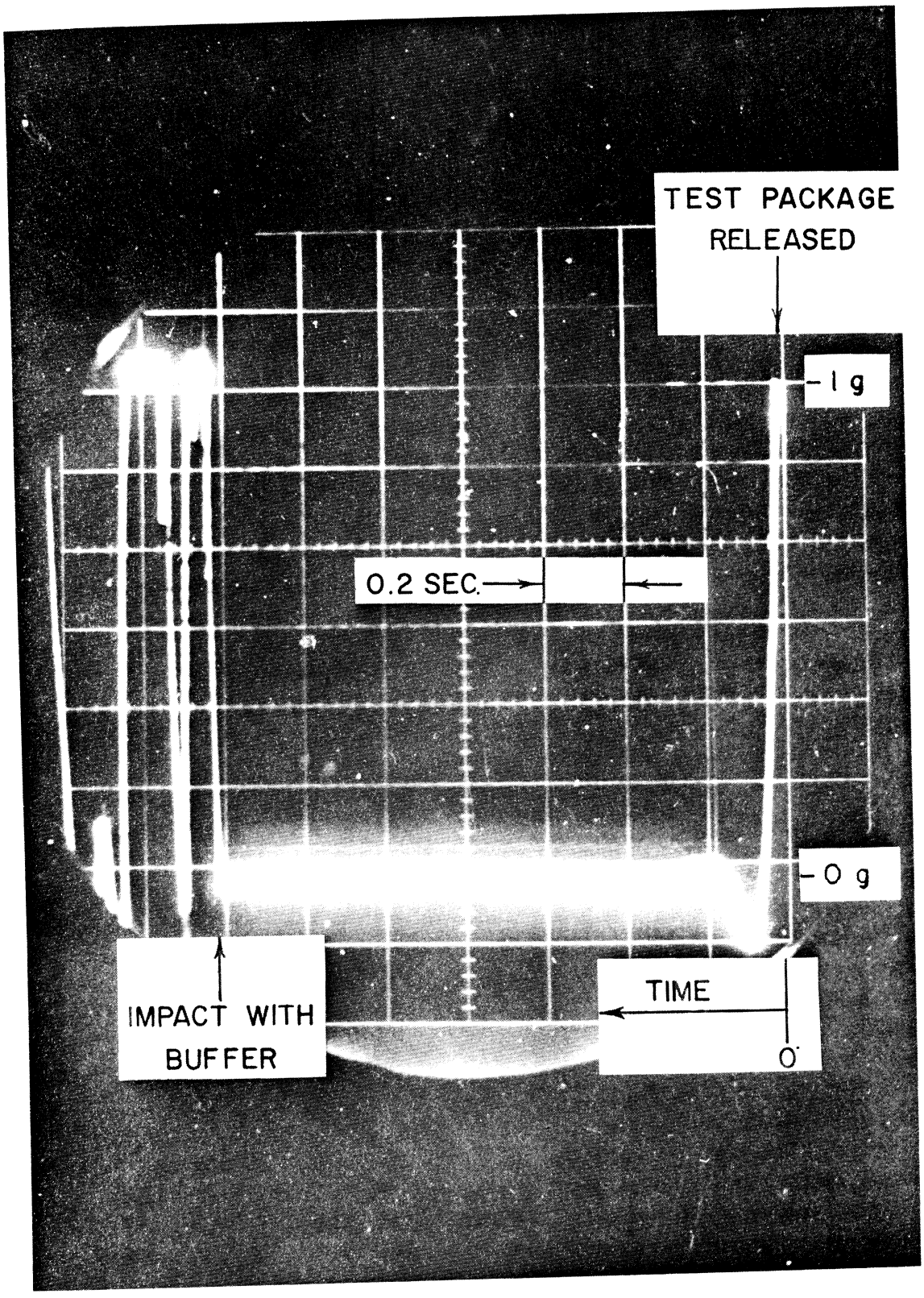

Fig. 13. Response of 0- to 1-g accelerometer with free fall.

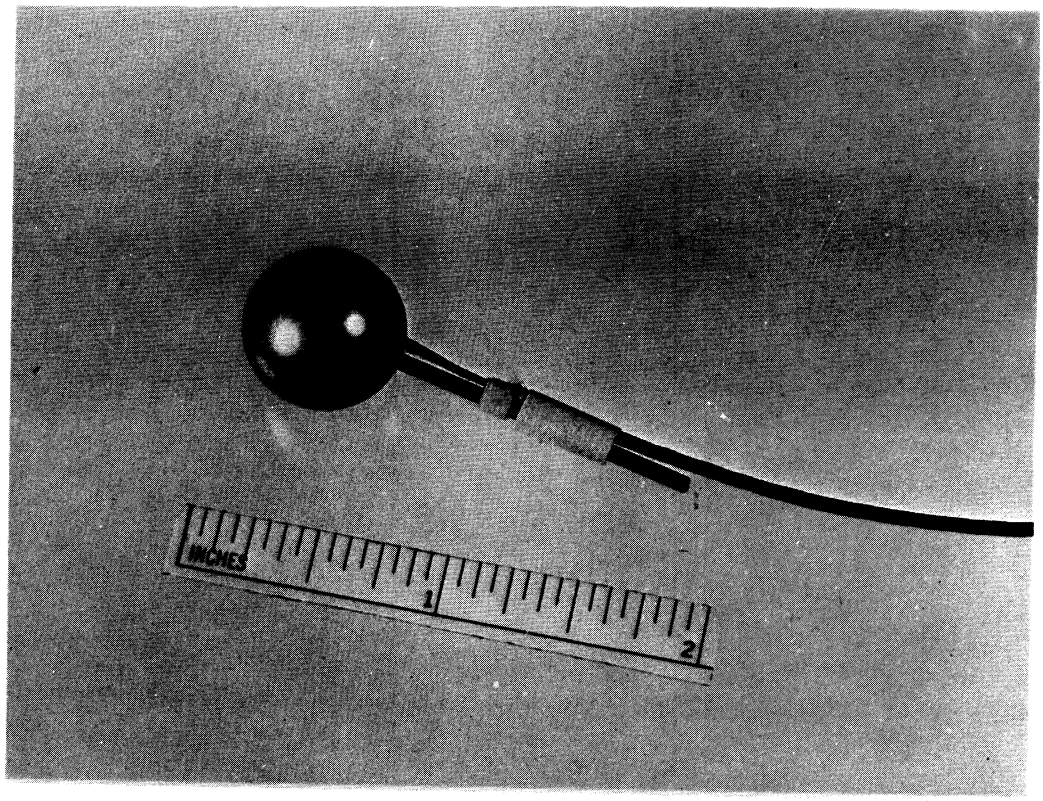

Fig. 14. 5/8-in.-OD aluminum sphere with 40-gage copper-constantan thermocouple at center.

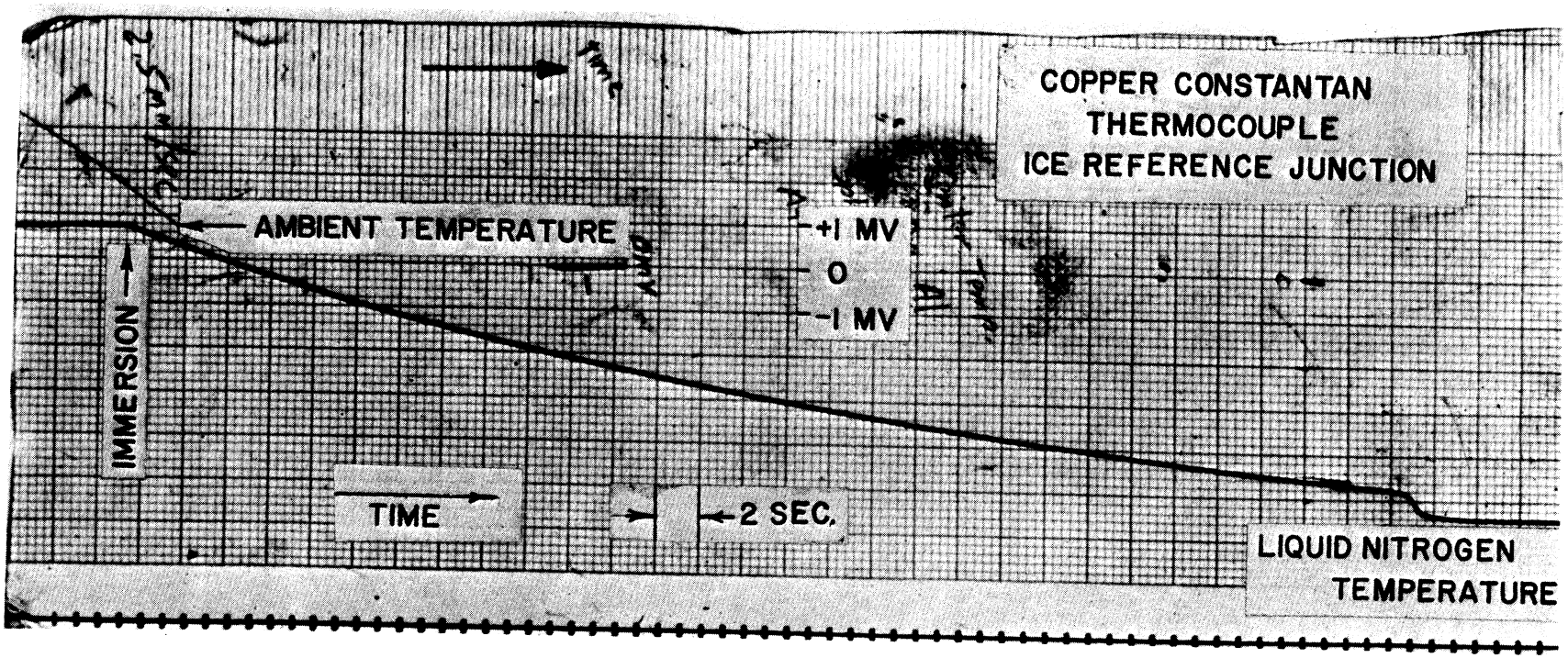

Fig. 15. Sanborn oscillographic record of center temperature of 5/8-in.-OD aluminum sphere plunged into liquid nitrogen with initial temperature at ambient a/g = 1.

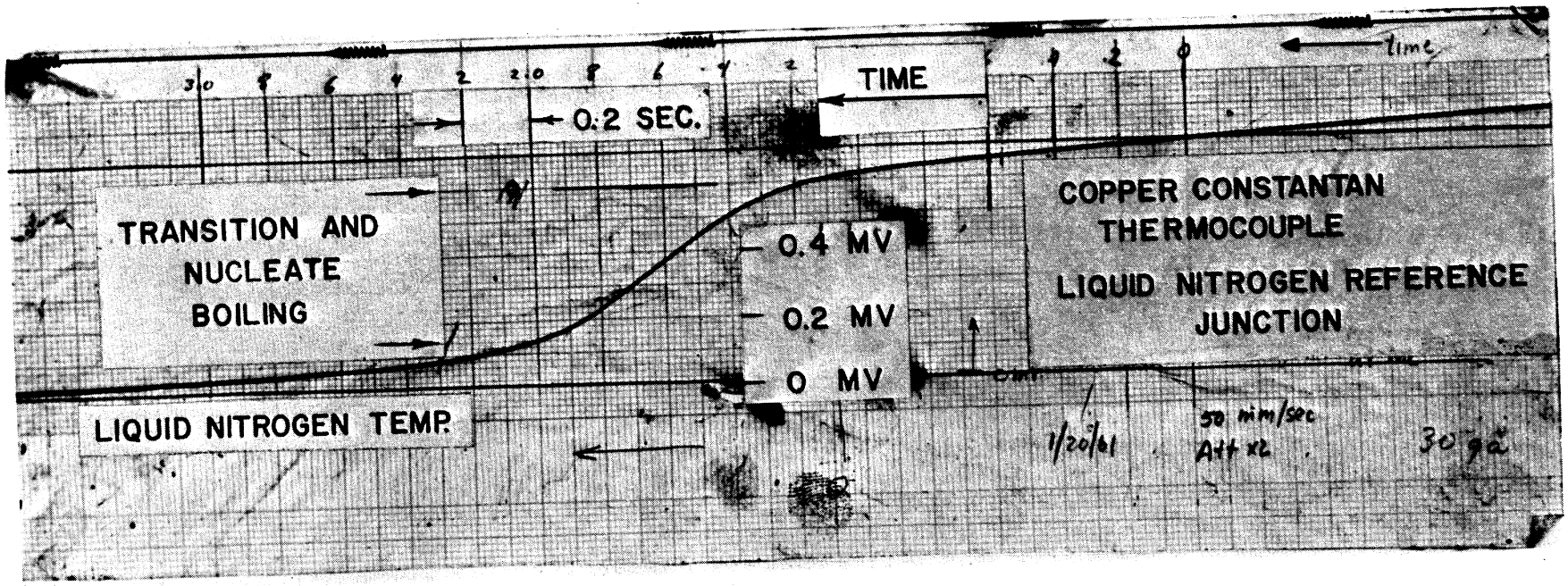

Fig. 16. Sanborn oscillographic record of center temperature of 5/8-in.-OD aluminum sphere as heat transfer mechanism passes through transition and nucleate boiling. a/g = 1.

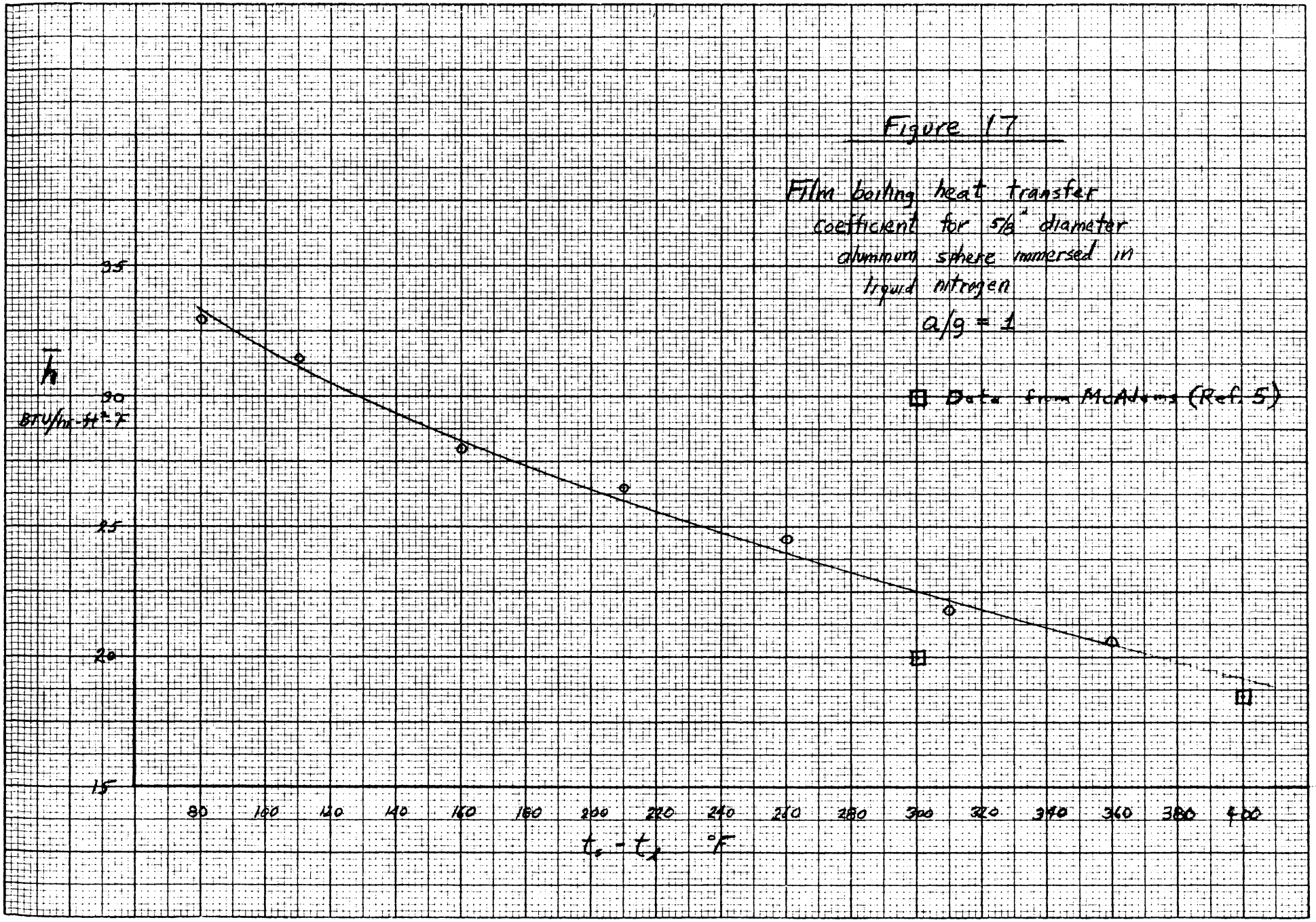
Figure 17
Film boiling heat transfer coefficient for 5/8" diameter aluminum sphere immersed in liquid nitrogen
a/g = 1
Data from McAdams (Ref. 5)
$\bar{h}$
BTU/hr-ft²-F
35
30
25
20
15
80
100
120
140
160
180
200
220
240
260
280
300
320
340
360
380
400
$t_s - t_l$ °F

FIG. 18

SPECIFIC HEAT OF ALUMINUM

Reference: CRYOGENIC ENGINEERING
by
R.B. SCOTT, VAN NOSTRAND CO., INC.

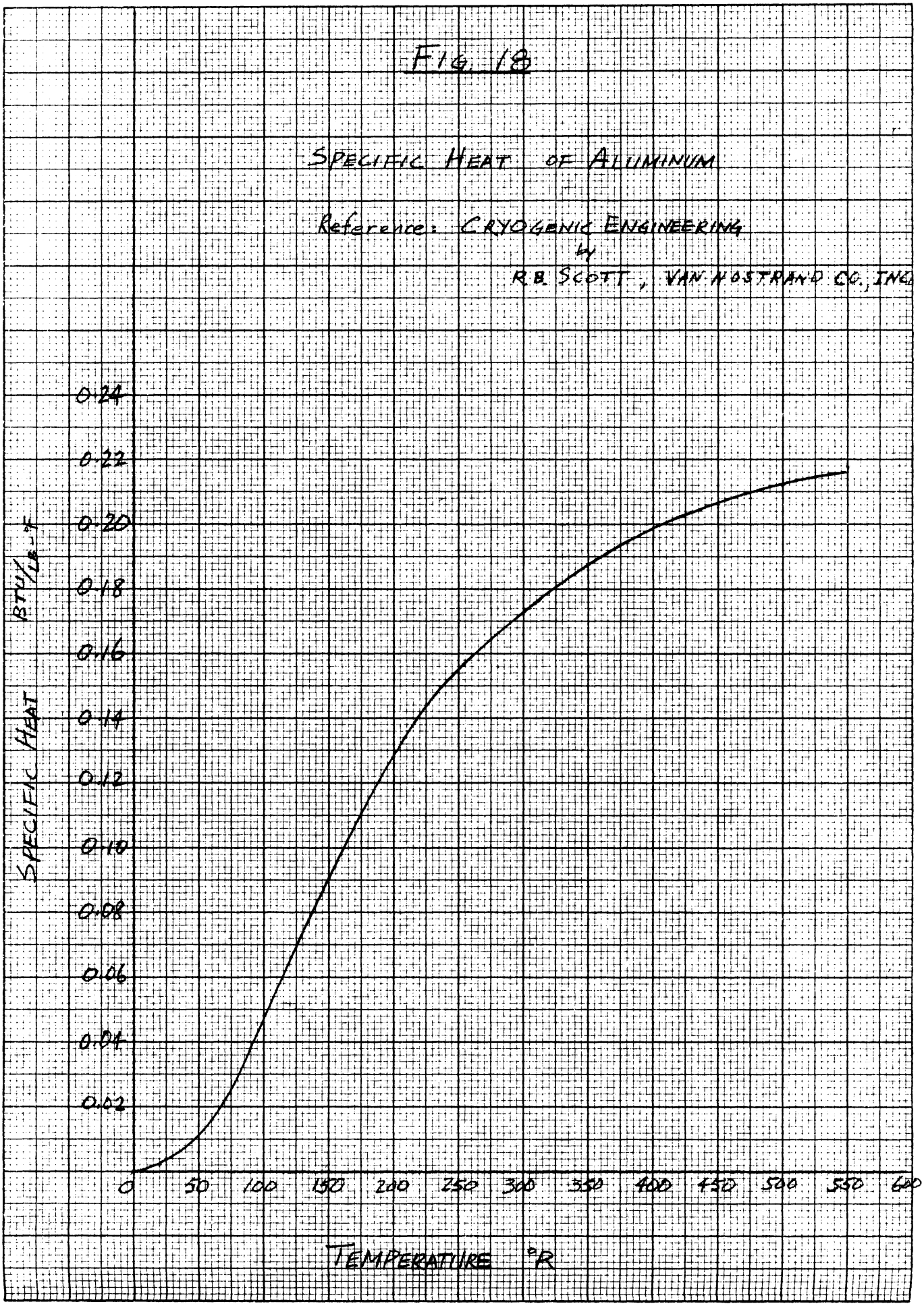

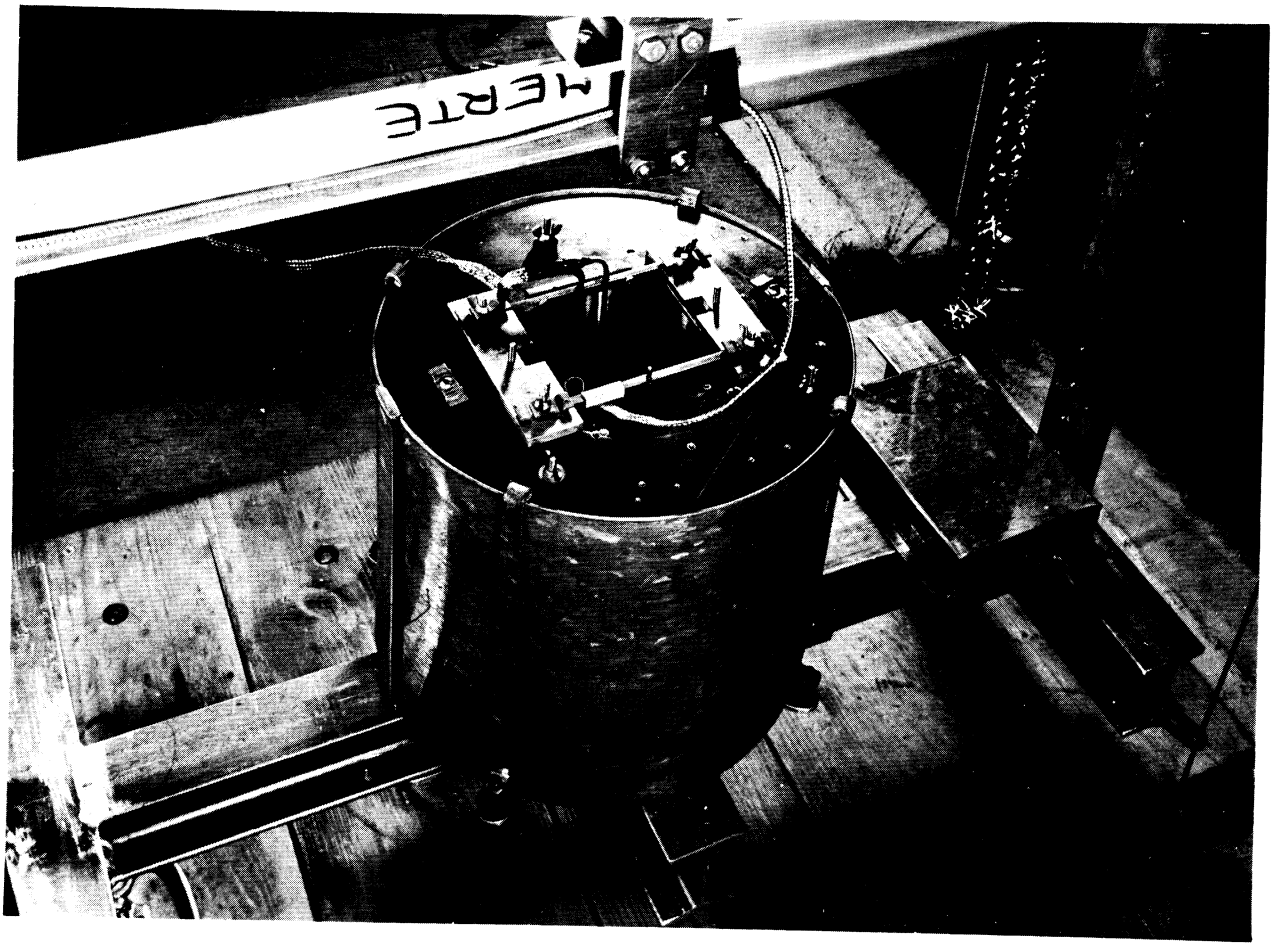

Fig. 19. View of insulated test vessel mounted on test platform.